IEEE Access
Multidisciplinary | Rapid Review | Open Access Journal

Received November 22, 2019, accepted December 5, 2019, date of publication December 10, 2019,
date of current version December 23, 2019.

*Digital Object Identifier 10.1109/ACCESS.2019.2958600*

# Vital Sign Signal Extraction Method Based on Permutation Entropy and EEMD Algorithm for Ultra-Wideband Radar

**DEGUI YANG, ZHENGLIANG ZHU, AND BUGE LIANG**
School of Aeronautics and Astronautics, Central South University, Changsha 410083, China

Corresponding author: Zhengliang Zhu (zzlcsu@foxmail.com)

This work was supported in part by the National Key Research and Development Program of China under Grant 2018YFC0810204.

**ABSTRACT** The noncontact measurement of vital sign signals is useful for medical care, rescuing disaster survivors from ruins and public safety. In this paper, a novel vital sign signal extraction method based on permutation entropy (PE) and ensemble empirical mode decomposition (EEMD) algorithm is proposed. The proposed algorithm analyzes the permutation entropy of radar-received pulses; the range between a human target and ultra-wideband (UWB) radar can be obtained by permutation entropy. Permutation entropy represents the complexity of signals, so we can use PE to select and recombine human life signals that are distributed in the adjacent distance gate. Moreover, EEMD algorithm is adopted to decompose the combined signal into intrinsic mode functions (IMF), and both the respiration and the heartbeat signals are reconstructed by IMF via reaching the energy threshold in the time domain. Experiments are carried out using UWB radar. Compared with traditional algorithms, the proposed algorithm can be used to extract the range and frequency information of human targets efficiently and accurately.

**INDEX TERMS** Vital sign signal, ultra-wideband (UWB) radar, ensemble empirical mode decomposition (EEMD), permutation entropy (PE).

## I. INTRODUCTION

In recent years, the needs of human noncontact measurement of vital signs by using radar is increasing; relevant research results are applied to the medical care of patients [1], [2], the rescue of disaster survivors from ruins [3], [4], public safety [5]–[7], and so on. Ultra-wideband (UWB) radar effectively measures human vital signs because of its high resolution, low power consumption, strong antijamming capability, etc. Much work has been done by many scholars on human vital sign detection [8]–[18].

In [8], the time-domain signal of UWB radar was analyzed using a morphological filtering method to extract the human heart rate. An improved arctangent demodulation technique was proposed to determine the frequency of human micromotion based on a multiple frequency accumulation method [9]. In [10], human respiratory motion detection based on a short-time Fourier transform (STFT) and singular value decomposition (SVD) was studied with respect to three different media. In [11], quasiperiodic echoes in the slow-time dimension were analyzed based on the characteristics of impulse radio UWB radar vital sign signals, and a vital sign signal extraction algorithm based on multiple higher-order cumulants was introduced. In [12], the finite difference time domain numerical simulation approach and synthetic computational experiments were used to design simulation models of human vital sign detection under collapsed building debris caused by earthquakes; advanced signal processing, such as source separation and empirical mode decomposition, was used to determine the location of human targets. In [13], human heart-lung respirate was analyzed using a numerical simulation method. The Hilbert-Huang Transforms (HHT) was used to discriminate between different human respiratory states. In [14], nonstationary signals caused by moving targets and respiratory motion signals were separated by SVD to improve the detection performance of UWB radar in low signal-to-noise-and-clutter ratio (SNCR) conditions. In [15], empirical mode decomposition (EMD) was adopted to adaptively decompose radar signals into intrinsic mode functions (IMF). By calculating the energy spectrum characteristics of each IMF, the respiratory and heartbeat signals are reconstructed in the time domain. Based on the idea in [15], ensemble empirical mode decomposition (EEMD) was performed to reduce modal aliasing. Meanwhile, the high-order

The associate editor coordinating the review of this manuscript and approving it for publication was Chengpeng Hao.

  

cumulants of reconstructed signals were calculated to improve measurement accuracy [16]. In [17], EEMD was used to improve the signal-to-noise ratio of echo signals. Continuous wavelet transforms (CWT) was used to separate the heartbeat and respiratory signals from radar-received signals, but the performance of the algorithm depended on the selection of the wavelet basis. In [18], variational mode decomposition (VMD) was used to suppress mode aliasing, but decomposition levels needed to be determined according to the number of targets in the detection scenario. The proposed algorithms mentioned above can accurately measure human vital signs, but the algorithms depend on radar data accumulated over a long period.

In traditional algorithms for human vital sign extraction, the respiratory and heartbeat frequency are obtained by Fourier spectrum analysis of the single-frame signal. However, when the sampling frequency is fixed, the longer the sequence participated, the better the spectrum. Therefore, we need long-term observation data; this need, however, reduces the efficiency of radar. To solve this problem, we propose a vital sign signal extraction method based on permutation entropy (PE) and an EEMD algorithm for UWB radar. PE is used to calculate the complexity of time-domain signals. By calculating the PE values of radar received-pulses along the fast-time direction, the distance between a human target and radar can be estimated according to PE values. Human vital sign signals are distributed on adjacent distance gates because 1. the radar transmitter has a certain trail; 2. the transverse width of the human thorax is nearly 30-40 centimeters, and multiple scattering points may exist on the thorax; and 3. the human body has a slight swing motion. By choosing and combining the signals on these distance gates based on PE values, more vital signs information can be obtained than single-frame signals, and the observation time can be reduced. EEMD is adopted to adaptively decompose the combined radar echo signal into IMF. According to the energy ratio of each IMF, the respiratory and heartbeat signals are extracted. The experimental results show that the proposed algorithm can effectively extract human vital sign signals quickly.

This paper is organized as follows: In section I, the application scenario of noncontact measurement of UWB radar and the status of current research vital sign signal processing algorithms are introduced. In section II, the UWB vital sign signal model is analyzed. In section III, the proposed algorithm is presented in detail. In section IV, the experimental setup and UWB radar system are introduced, and the results are analyzed. Section V is the conclusion of the paper.

## II. UWB RADAR VITAL SIGN SIGNAL MODEL

When UWB radar detects vital sign signals, radar echo signals mainly include human-generated modulation signals with micromotion such as breathing, heartbeats, and surrounding environmental noise signals. In this paper, we assume that in detection scenarios, in addition to human micromotion (i.e., breathing and heartbeat motion), other objects are stationary. Therefore, the impulse response of signal propagation can be expressed as [19]

$$h(t, \tau) = A_v\delta(\tau - \tau_v(t)) + \sum_s A_s\delta(\tau - \tau_s) \tag{1}$$

where $\tau$ denotes fast time, $t$ denotes slow time, $A_v\delta(\tau - \tau_v(t))$ is human micromotion, $A_v$ denotes the amplitude of human micromotion echo signals, $\tau_v(t)$ is the time delay generated by human micromotion, $\sum_s A_s\delta(\tau - \tau_s)$ is the stationary objects in the surrounding environment, $A_s$ denotes the amplitude of echo signals from stationary objects, and $\tau_s$ is the time delay generated by stationary objects.

Human respiratory and heartbeat activity lead to periodic changes in the chest cavity. Assuming that a human is target perpendicular to the radar line of sight, the human target is located at a fixed distance $d_0$, and the chest cavity change is $\Delta d(t)$, then $\tau_v(t)$ can be expressed by

$$\begin{aligned}\tau_v(t) &= \frac{2(d_0 + \Delta d(t))}{v} \\ &= \frac{2(d_0 + d_r cos(2\pi f_r t) + d_h cos(2\pi f_h t))}{v} \\ &= \tau_0 + \tau_r cos(2\pi f_r t) + \tau_h cos(2\pi f_h t)\end{aligned} \tag{2}$$

where $v$ is the propagation velocity of an electromagnetic wave (i.e.,$v = 3 \times 10^8 m/s$), $\tau_0 = \frac{2d_0}{v}$ is the time delay of the human, $\tau_r = \frac{2d_r}{v}$, $\tau_h = \frac{2d_h}{v}$ is the time delay of respiration motion and heartbeat motion respectively, $f_r$ is the frequency of the respiration, and $f_h$ is the frequency of the heartbeat.

We assume that the transmission impulse signal of the UWB radar is $p(\tau)$; therefore, the echo signals received by the receiving antenna can be written as

$$\begin{aligned}R(t, \tau) &= p(\tau) \otimes h(t, \tau) \\ &= A_v p(\tau - \tau_v(t)) + \sum\nolimits_s A_v p(\tau - \tau_s)\end{aligned} \tag{3}$$

where $\otimes$ represents a convolution operation.

Discretize equation (3) along both the slow-time direction and fast-time direction; then, we can obtain $M \times N$ matrix

$$\begin{aligned}R_{M\times N} &= R(\tau = mT_f, t = nT_s) \\ &= \sum\nolimits_s p(mT_f - \tau_s) + A_v p(mT_f - \tau_v(nT_s))\end{aligned} \tag{4}$$

where $t = nT_s; n = 0, 1, 2, \ldots, N-1, N \in Z^+$; $T_s$ represents the sampling interval along the slow-time direction; $\tau = mT_f; m = 0, 1, 2, \ldots, M-1, M \in Z^+$; and $T_f$ represents the sampling interval along the fast-time direction.

$R_{M\times N}$ denotes the radar echo data matrix of the human vital sign signal. If the matrix is processed properly, the vital sign signal can be extracted. Figure 1 illustrates the vital sign signal model of the received data without clutter. The slow-time dimension represents the observation time, i.e., the number of received pulses. The fast-time dimension represents the detection range of the radar. The dotted line in Figure 1 is the location scope of the human targets. The waveform of the target position will change periodically in the slow-time direction due to periodic behaviors, such as respiratory and heartbeat motion.

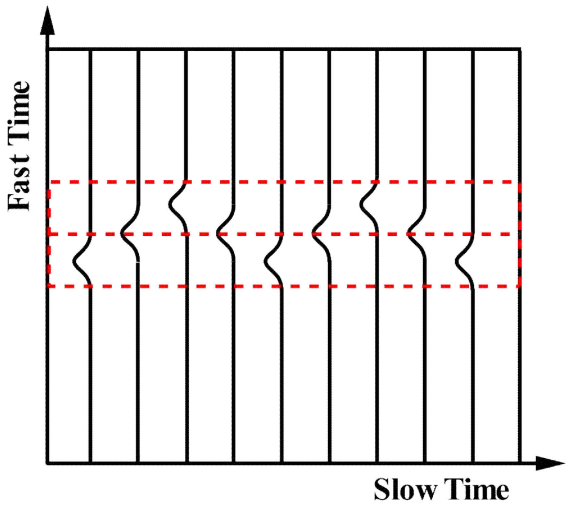


**FIGURE 1.** An illustration of the vital sign signal model.

## III. PROPOSED ALGORITHM

In this section, the proposed algorithm is introduced in detail. The algorithm includes three parts: signal preprocessing, distance detection and echoes selection, and vital sign signal extraction. The flowchart of this algorithm is given in Figure 2.

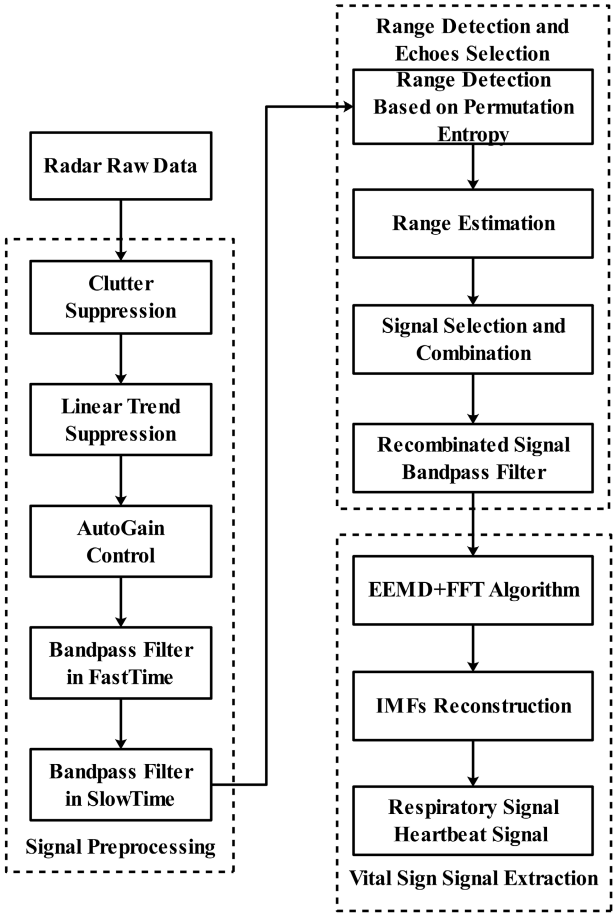


**FIGURE 2.** Flowchart of the proposed algorithm.

### A. SIGNAL PREPROCESSING

In actual detection, human vital sign signals are covered by strong background clutter signals. Denote Ωas the radar received pulses matrix after signal pre-processing.

#### 1) CLUTTER SUPPRESSION

The echo from stationary objects in the detection scene can be approximated to a direct current (DC) component. The expression can be written as

$$\mu = \frac{1}{M \times N} \sum_{m=1}^{M} \sum_{n=1}^{N} R[m, n] \tag{5}$$

Then the results of removing static clutters can be obtained

$$\bar{R}_{M\times N} = R_{M\times N} - \mu \tag{6}$$

To remove as much background clutter as possible, we use an exponential weighting cancellation method to estimate the amount of background clutter; take the $n_1$th frame echo as an example [20]

$$\Im[m, n] = \alpha\Im[m, n-1] + (1-\alpha)\bar{R}[m, n] \tag{7}$$

where $\alpha$ is a weighting factor, $\alpha \in (0, 1)$,$\Im[m, 1] = \bar{R}[m, 1]$, and $\Im[m, n-1]$ denotes the background clutter which estimated from the previous echoes. Then the echo matrix after clutter suppression can be written as

$$\widehat{\Omega}_{M\times N} = \bar{R}_{M\times N} - \Im \tag{8}$$

#### 2) LINEAR TREND SUPPRESSION

The unstable amplitude of the transmitting unit is caused by thermal noise and time drift; this unstable amplitude leads to the linear trend of the radar received data along the slow time. Therefore, the least-squares fit method is used to estimate and subtract

$$\Omega = \widehat{\Omega}^T - w(w^T w)^{-1} w^T \cdot \widehat{\Omega}^T \tag{9}$$

where $w = [w_1, w_2]$, $w_1 = [0, 1, \ldots, M-1]^T$; and $w_2 = [1, 1, \ldots, 1]^T$.

#### 3) SIGNAL-TO-NOISE RATIO (SNR) IMPROVEMENT

High-frequency noise is caused by a heavy oversampling backscatter signal [11]. Therefore, a Butterworth bandpass filter is designed in range direction to improve the SNR. The mean filter is used to eliminate low-frequency and high-frequency noise in the slow-time dimension [21]. The human amplitude in the radar-received pulse is related mainly to the cross section of the human body and the relative distance between human target and the radar. The multipath effect in the actual test scenario also interferes with the target echo. Therefore, auto gain control (AGC) is used to enhance the weak human vital sign signal to further improve SNR [22]. The AGC algorithm enhances the human life signal in the range dimension and calculates the corresponding gain coefficient according to the energy in selected time

window $2\lambda+1$, thereby achieving adaptive control. Take the $n_1$th frame echo signal $r(\tau, n_1)$ as an example

$$g_{mask}(\tau_i, t) = \frac{2\lambda+1}{\sqrt{\sum_{k=i-\lambda}^{i+\lambda} r(\tau_k, t)^2}} \tag{10}$$

$$r_E(\tau, t) = g_{mask}(\tau, t) \times r(\tau, t) \tag{11}$$

where $g_{mask}(\tau_i, t)$ represents signal gain coefficients and $r_E(\tau, t)$ is the enhanced signal after AGC.

### B. RANGE DETECTION AND ECHOES SELECTION

To detect the range of the human target in the radar echo matrix $\Omega$, the statistical characteristics (such as kurtosis, standard deviation and variance) in the range dimension are analyzed [18], [23], [24]. In this paper, the signal complexity of the target region and the nontarget region are different in the slow-time dimension of radar-received pulses, so permutation entropy is adopted to detect the position of the human target. Permutation entropy was proposed by Christoph Bandt in [25], to detect randomness and dynamics mutations of time series. PE can effectively detect and amplify the dynamic changes of time series such as signals, and has the properties of simple calculation [26] (the computational complexity is O(n)) and strong anti-interference. The principle of PE is as follows.

We suppose that at the fast time $m_1$, time series $X[m_1, i] = \{x(1), x(2), \ldots, x(i)\}, i = 1, 2, 3, \ldots, N, X \in \Omega_{M\times N}$ can be obtained and reconstruct its phase space matrix

$$\begin{bmatrix} x(1) & x(1+\tau_d) & \ldots & x(1+(q-1)\tau_d) \\ x(2) & x(2+\tau_d) & \ldots & x(2+(q-1)\tau_d) \\ x(j) & x(j+\tau_d) & \ldots & x(j+(q-1)\tau_d) \\ \ldots & \ldots & \ldots & \ldots \\ x(K) & x(K+\tau_d) & \ldots & x(K+(q-1)\tau_d) \end{bmatrix}, \quad j = 1, 2, 3, \ldots, K \tag{12}$$

where $q$ represents the embedding dimensions, $\tau_d$ is the time delay, and $K = N - (q-1)\tau_d$. Each row in the phase space matrix can be regarded as a reconstructed component. Reorganizing $j_{th}$ reconstructed component in ascending order, $j_1, j_2, \ldots, j_q$ represents the index of elements in the phase space matrix.

$$x(i+(j_1-1)\tau_d) \le x(i+(j_2-1)\tau_d) \le \ldots \le x(i+(j_q-1)\tau_d) \tag{13}$$

If equal values exist in the reconstructed component

$$x(i+(j_1-1)\tau_d) = x(i+(j_2-1)\tau_d) \tag{14}$$

Then, sorted according to the value of $j_1, j_2$

$$x(i+(j_1-1)\tau_d) \le x(i+(j_2-1)\tau_d) \tag{15}$$

Then, for each row data in the phase matrix that are reconstructed any by any time series, we can obtain a set of symbol sequences

$$S(l) = (j_1, j_2, \ldots, j_q) \tag{16}$$

where $l = 1, 2, \ldots, k, k \le q!$.

A total of $q!$ symbol sequences map from the phase space. If the probability of each symbol sequence $P_1, P_2, P_3, \ldots, P_k$ is calculated for a time series, the permutation entropy of $k$ different symbol sequences can be defined in the form of Shannon entropy

$$H_p(q) = -\sum_{j=1}^{k} P_j \ln P_j \tag{17}$$

In (17), when $P_j = \frac{1}{q!}$, the maximum of $H_p(q)$ is reached; i.e., $\max\{H_p(q)\} = \ln(q!)$. Therefore, we can use the maximum for normalization.

The permutation entropy algorithm does not rely on the specific value of the time series but analyzes the data by comparing the adjacent data. Some parameters (such as the length of data $L$,embedding dimension $q$ and time delay $\tau_d$) for calculating the permutation entropy need to be predetermined [27]–[29]. Bandt recommended that the embedding dimension $q \in [3, 7]$ for calculating PE in [25] because if $q = 1$ or 2, there are few states in the reconstructed vector, the permutation entropy loses its validity, and the mutation of the time series cannot be detected. Conversely, if $q > 7$, it takes more computation time. Meanwhile, the reconstruction of the phase space leads to a homogeneous time series, and it is difficult to characterize the subtle changes of the signals. Take a random signal with a length of 240 as an example. Figure 3 shows the relationship between the PE values and the embedding dimension under different time delays. As shown in Figure 3, the time delay has less influence on PE values. Next, in this paper, we set time delay $\tau_d$ to 1. According to [28], to achieve a reliable PE measurement, the signal length $L$ must fulfill $L >> q!$. PE values according to differences in sequence length are given in Figure 4. For random signals with lengths of 80, 160, 240, 320 and 400, the corresponding PE values are calculated and denoted as $PE_1, PE_2, PE_3, PE_4, PE_5$, respectively.

Table 1 shows the differences in the PE of random signals based on different lengths and embedding dimensions. According to the results of Table 1, when the embedding dimension q = 3 and time delay $\tau_d = 1$, the permutation entropy of a random signal with data length of 80 differs from the entropy of a random signal with a data length of 160 by 0.0024, and the permutation entropy of a data length 320 differs from the permutation entropy of a random signal with a data length of 240 by 0.0023. Therefore, it is appropriate to set the data length to 80.

**TABLE 1. Differences in the pe of random signals based on different lengths and embedding dimensions.**

| $q$ | 3 | 4 | 5 | 6 | 7 |
|---|---|---|---|---|---|
| $PE_2 - PE_1$ | 0.0024 | 0.0250 | 0.1104 | 0.0832 | 0.0828 |
| $PE_3 - PE_2$ | 0.0006 | 0.0047 | 0.0229 | 0.0683 | 0.0502 |
| $PE_4 - PE_3$ | 0.0023 | 0.0022 | 0.0175 | 0.0367 | 0.0298 |
| $PE_5 - PE_4$ | 0.0016 | 0.0049 | 0.0072 | 0.0232 | 0.0258 |

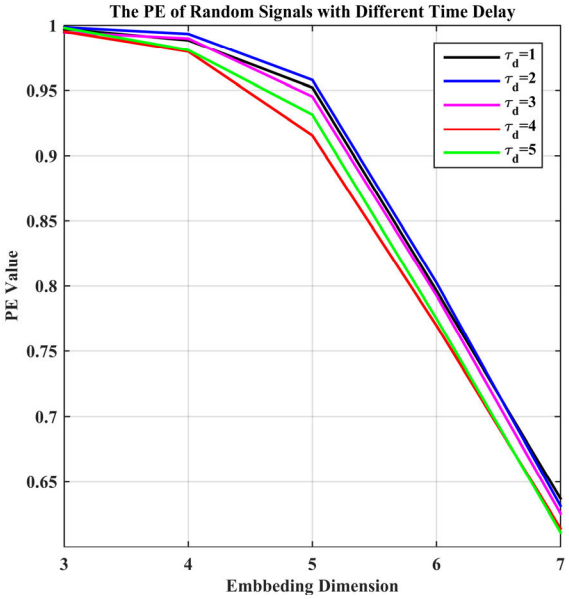


**FIGURE 3.** The PE of random signal with different time delays.

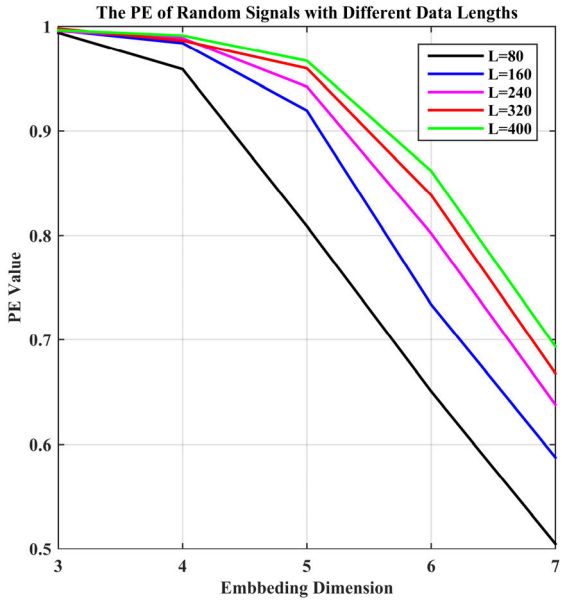


**FIGURE 4.** The PE of random signals with different data lengths.

According to the analysis above, we can conclude that PE is insensitive to the length of random signals when q = 3 and $\tau_d = 1$. Therefore, in this study, the parameters of permutation entropy are set as follows: the embedding dimension is 3, the signal length is 80 and the time delay is 1.

The value of PE indicates the randomness of the time series: the lower the PE value is, the more regular the time series becomes. Changing the value of PE can reflect and amplify the subtle change of the time series. In the radar-received echoes matrix $\Omega_{M\times N}$, the PE value of the human target region has relatively regular vital sign signals, so the corresponding PE value of the human target region is low, and the target position $P_{pos}$ can be determined by searching the minimum value index of the PE value. Then, the range information of targets can be given by

$$Range = \frac{v \times P_{pos} \times T_f}{2} \tag{18}$$

where $v = 3\times10^8 m/s$ and $T_f$ represents the sampling interval in the fast-time dimension.

In traditional algorithms (for example, variable points Fourier transforms) for detecting the vital sign signals, the respiratory and heartbeat frequency ware estimated by spectrum analysis of the single-frame signal accumulated in the slow-time dimension. However, when the sampling frequency is fixed, the longer the single-frame signal is, the better the spectrum is. Therefore, we need long-term observation data (approximately 20 seconds); this requirement reduces the efficiency of UWB radar. In actual radar detection, radar-received pulses carrying vital sign information will distrust at adjacent distance gates. Based on PE values, we can make full use of the echoes distributed in adjacent distance gates to increase the signal length and improve radar efficiency.

Assume the longitudinal width of human chest $D_{tho}$; then, according to the sampling interval $T_f$ in the fast-time dimension, the number of points occupied by the human chest in the received pulse can be calculated; i.e.,$P_{tho} = \frac{2D_{tho}}{vT_f}$, where $v = 3 \times 10^8 m/s$. Denote the vital sign signal matrix as $\Psi$, which can then be expressed by

$$\begin{aligned} \Psi &= \Omega[(P_{pos} - P_{tho}/2) : (P_{pos} + P_{tho}/2), 1 : n] \\ 0 &\le P_{pos}, P_{tho} \le M \\ n &= 1, 2, \ldots, N \end{aligned} \tag{19}$$

By arranging the vital sign signal matrix in rows, we can obtain the vital sign signal vector $\xi$. Figure 5 shows a schematic diagram of this section algorithm.

### C. VITAL SIGN SIGNAL EXTRACTION BASED ON EEMD

An EMD algorithm can adaptively decompose the signal into a series of intrinsic mode functions and residual signals according to the characteristics of the signal:

$$x(t) = \sum_{i=1}^{n} IMF_i(t) + r_n(t) \tag{20}$$

The physical meaning of each IMF corresponds to the oscillation characteristics of different scales in the original signal. An IMF must satisfy the following conditions: (i) the number of zero-crossings and extreme values must be equal or differ at most by one; and (ii) at any point, the mean value of the upper and lower envelopes is zero. Each IMF is extracted by using an iterative shifting process [30].

To suppress mode mixing in EMD algorithm, an EEMD algorithm was proposed by Huang [31]. By adding Gaussian white noise to the original signal, the signal is continuous at different scales. EEMD algorithm suppress mode mixing better than EMD algorithm because after EMD algorithm,

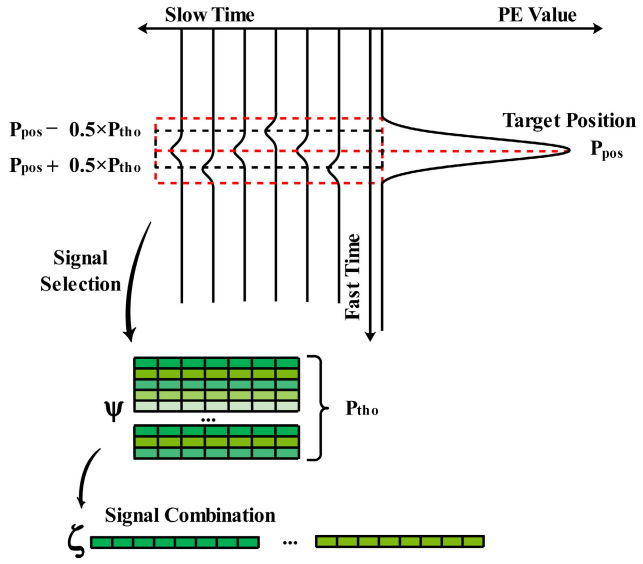


**FIGURE 5.** A schematic diagram of the section algorithm.

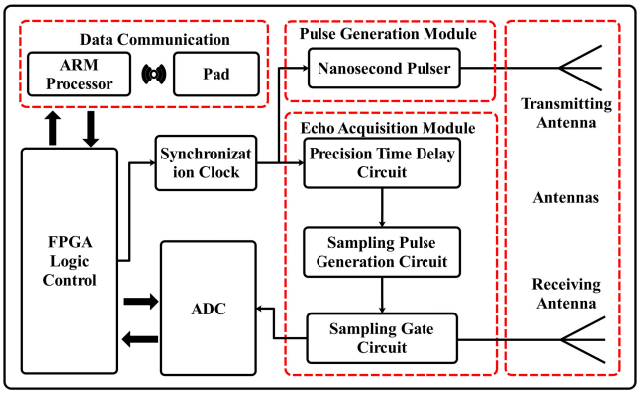


**FIGURE 6.** UWB radar system.

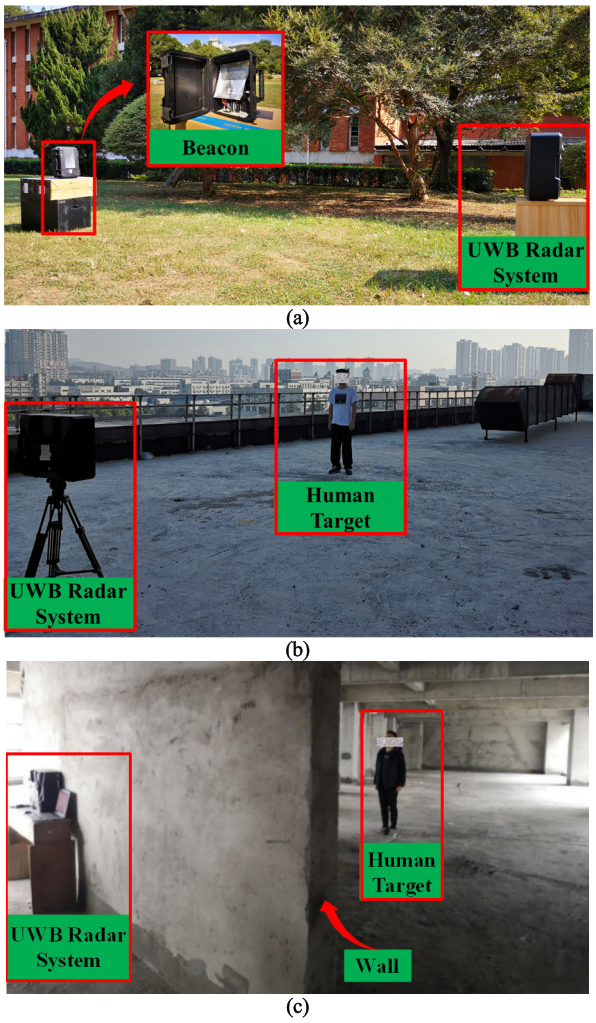


**FIGURE 7.** Experimental setup: (a) first experiment, (b) second experiment and (c) third experiment.

the added random white noise is uniform in the whole time-frequency space, and the different fluctuations of the original signal are automatically projected to the corresponding frequency fluctuations in the uniform time-frequency space established by the white noise. Since the white noise added by EMD decomposition is random and independent, the added random white noise is cancelled after averaging the corresponding IMF components. The details of the EEMD algorithm are as follows:

1. Add Gaussian white noise $n_i(t)$ to the original x($t$):

$$x_i(t) = x(t) + n_i(t) \quad i = 1, \ldots, I \tag{21}$$

where $n_i(t)$ represents the white Gaussian noise and $x_i(t)$ indicates the signal with Gaussian white noise.

2. Use the EMD algorithm on the signal $x_i(t)$ to obtain the corresponding IMF component.

3. Repeat steps 1-2 for $I$ times.

4. The average operation is performed on the IMF component by $I$ times EMD results, and the new IMF component can be obtained:

$$IMF_j(t) = \frac{1}{I}\sum_{i=1}^{I} IMF_{ji}, \quad i = 1, 2, \ldots, I \tag{22}$$

Finally, the results of the EEMD can be written as

$$x(t) = \sum_{j=1}^{n} IMF_j(t) + r_n(t) \tag{23}$$

where $r_n(t)$ is the residual signal.

The complete ensemble number $I$ is the key parameter of the EEMD algorithm; a large value of $I$can cause an expensive computation cost. For vital sign signal decomposition, we acknowledge that $I = 50$ by multiple experiments. Hence, in this study, the following parameters are set as follows: the complete ensemble number is set as $I = 50$, white Gaussian noise is added at 0.2 times the standard deviation of x($t$), and the G. Riling criterion is the stopping criterion of the EEMD algorithm .

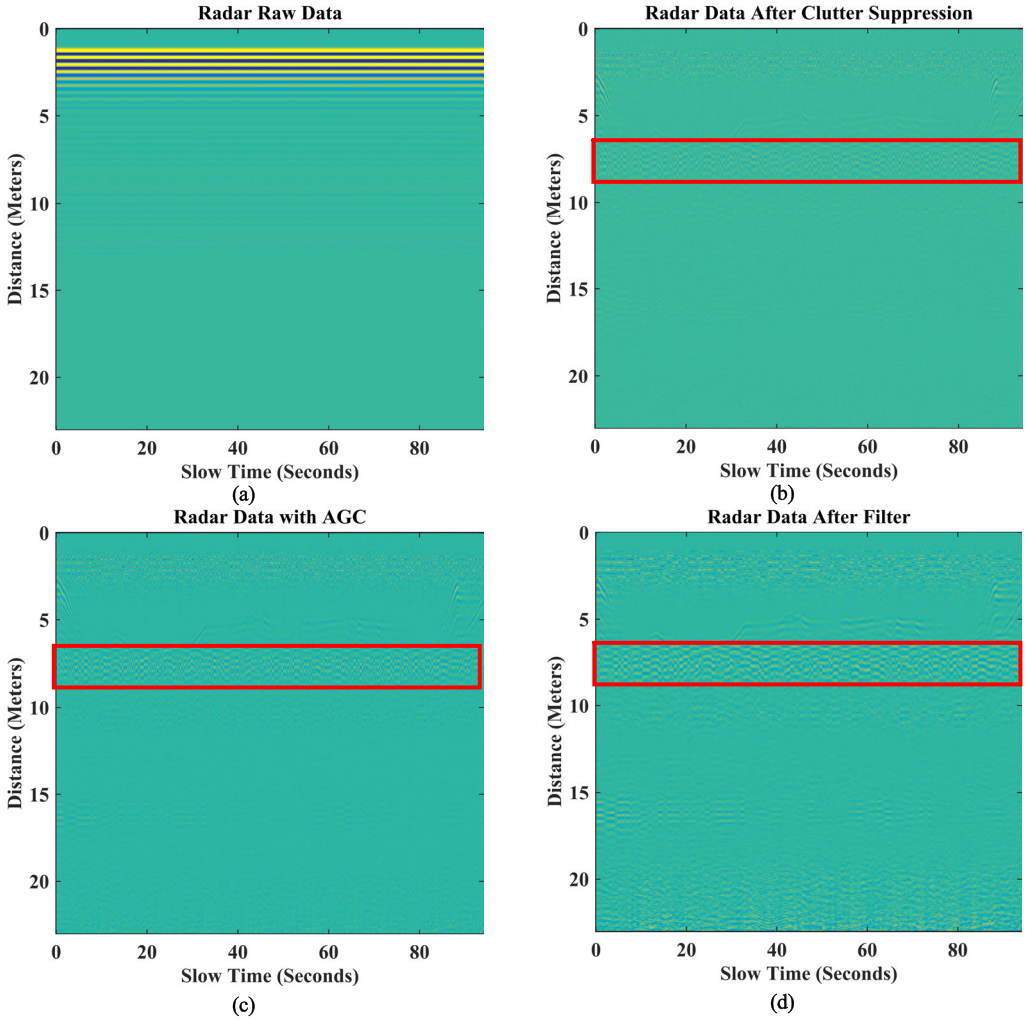


**FIGURE 8.** Signal preprocessing performance: (a) radar raw data, (b) radar data after clutter suppression, (c) radar data after AGC and (d) radar data after filter.

The EEMD algorithm is used to extract the respiratory and heartbeat signals based on the following principles: The important structure of the vital sign signal is concentrated in the low frequency range (the heartbeat frequency distribution range is 1-2.5 Hz, and the respiratory frequency distribution range is 0.2-0.8 Hz) [13]. Only the part of the IMFs that reflect the spectral structure of the vital sign signal is used to reconstruct the respiratory and heartbeat signals.

The signal $\xi$ is decomposed to $Z$IMFs; then, we can obtain a mode index set $\{z_1, z_2, z_3, z_4\} \in Z$. The selection rules of index set $\{z_1, z_2, z_3, z_4\}$ are as follows: Fourier transforms is performed on each of the IMFs, thereby computing the entire energy of each IMF in frequency domain $E(f)$, the energy of the respiration signal frequency range (0.2-0.8 Hz) $E_r(f)$ and the energy of the heartbeat signal frequency range (1-2.5 Hz) $E_h(f)$. $\delta_h$, $\delta_r$is the corresponding energy threshold. If the energy ratio of each IMF is larger than the energy threshold, we determine that the IMF can reconstruct the vital sign signals. The energy threshold is related to human posture. In [15], a conclusion was drawn from repeated experiments that the energy threshold value is 0.5 when the human target toward the radar. In this paper, we set the energy threshold to $\delta_h, \delta_r = 0.5$.

$$\begin{cases} z_1 = \arg\min\limits_{1\le z\le Z}[\frac{E_h(f)}{E(f)} \ge \delta_h] \\ z_2 = \arg\max\limits_{1\le z\le Z}[\frac{E_h(f)}{E(f)} \ge \delta_h] \\ z_3 = \arg\min\limits_{1\le z\le Z}[\frac{E_r(f)}{E(f)} \ge \delta_r] \\ z_4 = \arg\max\limits_{1\le z\le Z}[\frac{E_r(f)}{E(f)} \ge \delta_r] \\ \delta_h, \delta_r \in (0, 1) \end{cases} \tag{24}$$

Therefore, the heartbeat signal is reconstructed by $z_2 - z_1 + 1$ IMFs, and the respiratory signal is reconstructed by $z_4 - z_3 + 1$IMFs:

$$\begin{cases} s_h(t) = \sum\limits_{z=z_1}^{z_2} IMF_z(t) \\ s_r(t) = \sum\limits_{z=z_3}^{z_4} IMF_z(t) \end{cases} \tag{25}$$

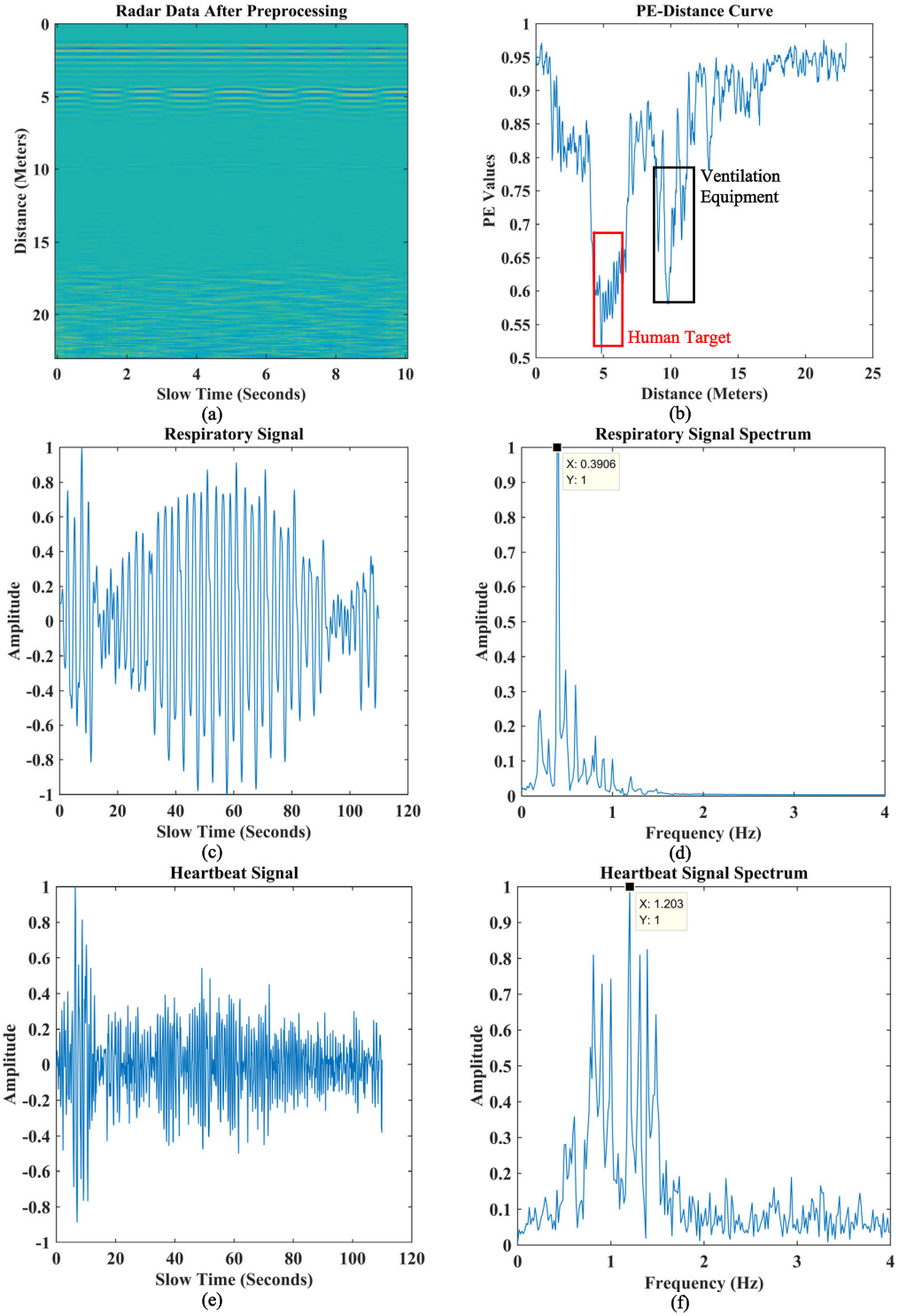


**FIGURE 9.** Vital sign signal extraction performance for a human target 5 meters from the radar in the second experiment: (a) radar data after preprocessing, (b) PE-distance curve, (c) reconstructed respiratory signal, (d) respiratory signal spectrum, (e) reconstructed heartbeat signal, and (f) heartbeat signal spectrum.

## IV. EXPERIMENT AND RESULTS ANALYSIS

### A. UWB RADAR SYSTEM AND EXPERIMENTAL SETUP

The composition of the UWB radar is shown in Figure 6. The UWB radar system was independently developed by the School of Aeronautics and Astronautics of Central South University. The pulse signal generating module generates a trigger pulse with a pulse repetition frequency of 400 KHz. After the transmitted signal is scattered by the target,

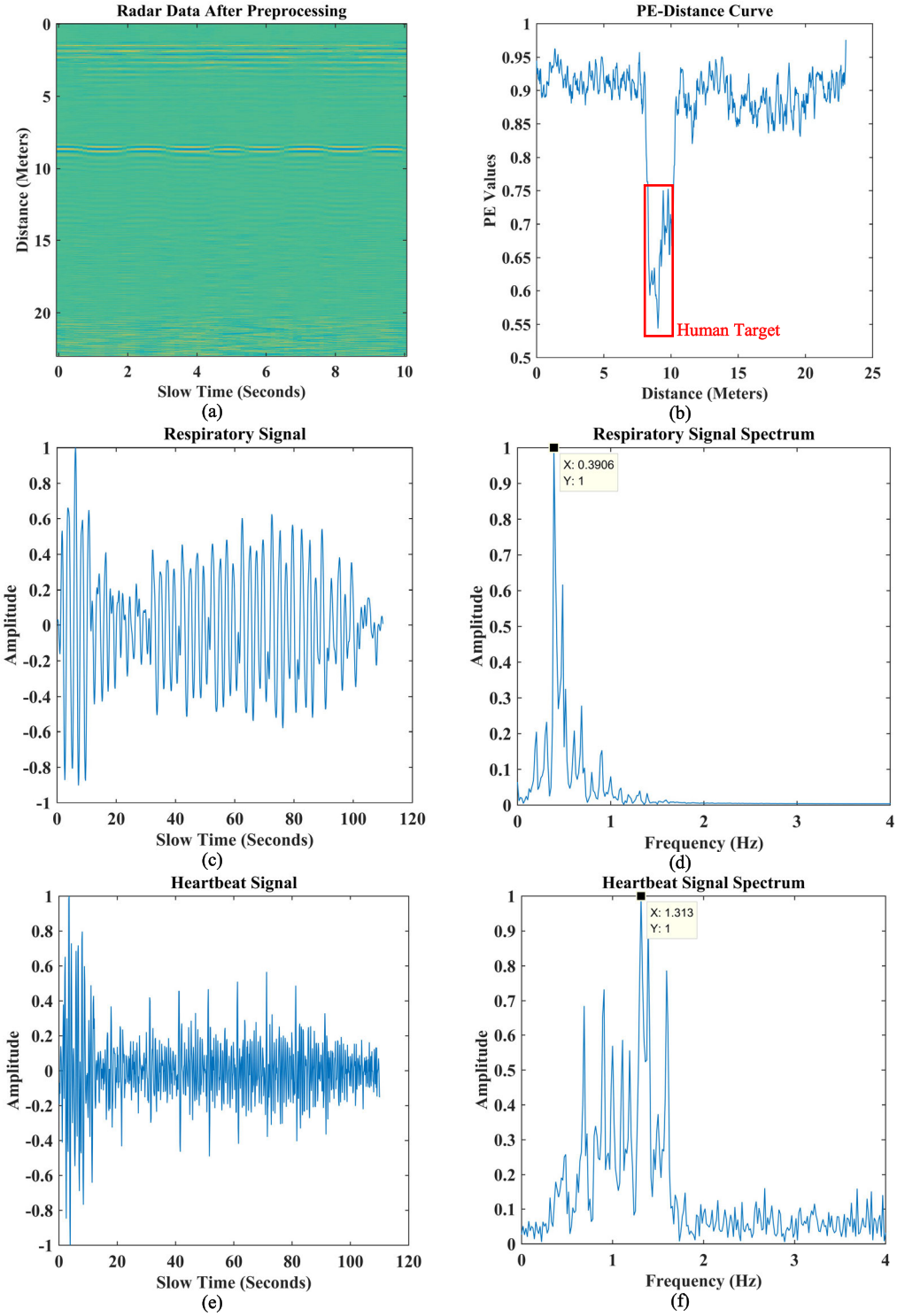


**FIGURE 10.** Vital sign signal extraction performance for a human target 9 meters from the radar in third experiment, (a) radar data after preprocessing, (b) PE-distance curve, (c) reconstructed respiratory signal, (d) respiratory signal spectrum, (e) reconstructed heartbeat signal, and (f) heartbeat signal spectrum.

the signals are sampled by the echo acquisition module, and then converted into digital signal by an analog-to-digital converter (ADC) and stored by a field programmable gate array (FPGA). The real-time sampling frequency of the ADC is 400 KSa/s. By using the equivalent sampling method, the equivalent sampling frequency can reach 5 GSa/s. Bow-tie antennas are used in the UWB radar system. Table 2 shows the parameters of this system.

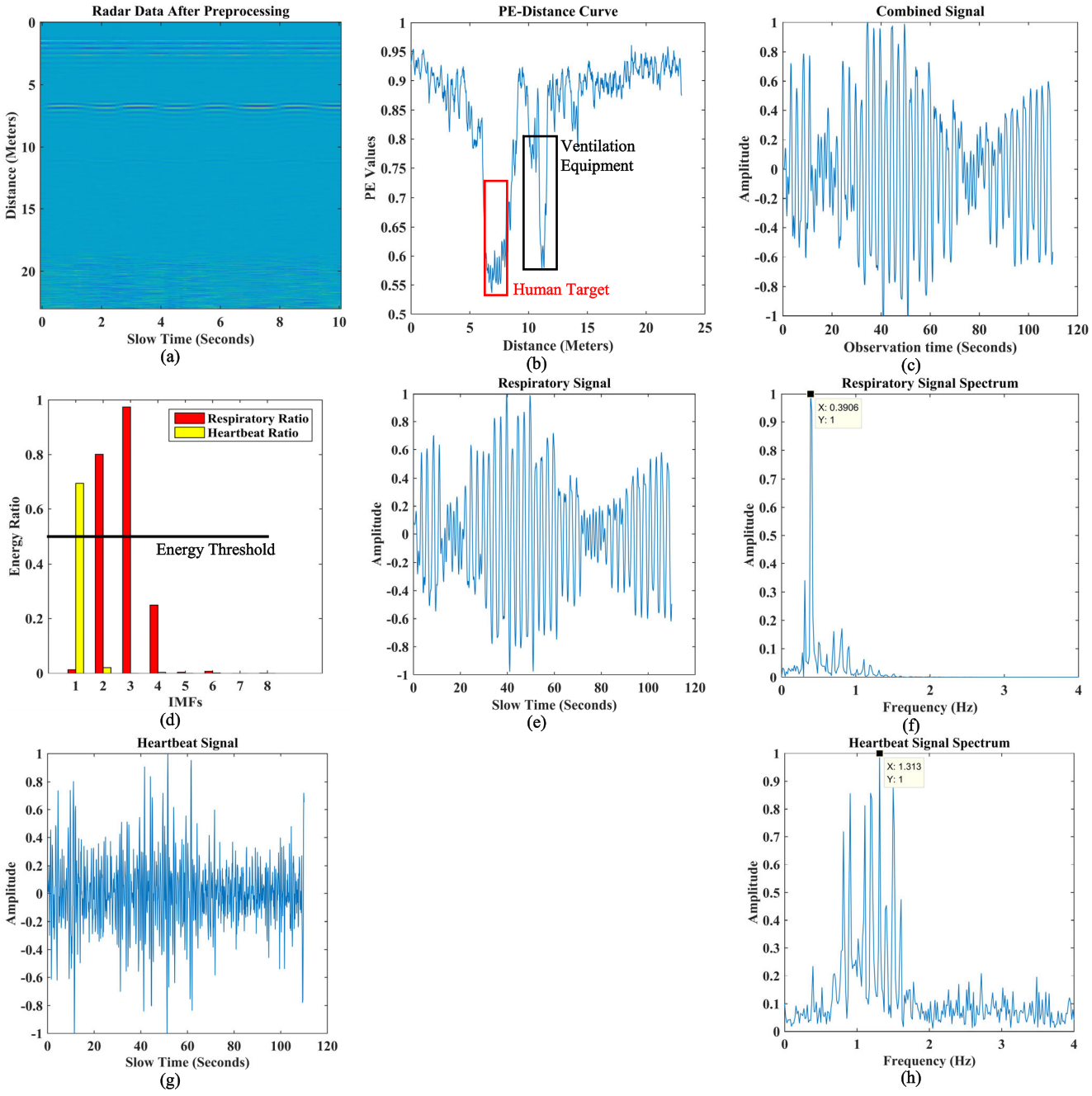


**FIGURE 11.** The presentation of the proposed algorithm for a human target 7 meters from the radar in the second experiment: (a) radar data after preprocessing, (b) PE-distance curve, (c) combined signal, (d) energy ratio of IMFs, (e) reconstructed respiratory signal, (f) respiratory signal spectrum, (g) reconstructed heartbeat signal, and (h) heartbeat signal spectrum.

To validate the effectiveness of the proposed algorithm, experiments are designed based on a UWB radar system. Figure 7 are the experimental scenarios. The first experiment was carried out in the back of the Democratic Building of Central South University. A beacon with a vibration frequency of 0.2 Hz was used to simulate the respiratory motion. The beacon is surrounded by plants such as weeds and is 7 meters away from the radar. The second experiment was conducted on the roof of a commercial office building. Metal railings and ventilation equipment on the rooftop may have affected the accuracy of the extraction of vital sign signals. The distance between the volunteer and the radar is 5 meters and then 7 meters. The third experiment was carried out in an indoors office building in Changsha; the volunteer is 9 meters away from the radar, and the wall (which is composed of brick and concrete) has a thickness of 20 centimeters. The volunteer participating in the experiment is a healthy adult male student (170 cm, 60 kg). The radar is 1.5 meters above

**TABLE 2. The parameters of the UWB radar system.**

| Parameters | Value |
|---|---|
| Operating mode | Impulse |
| Center frequency | 500MHz |
| Pulse width | 2ns |
| Sampling points | 768 |
| Sampling interval by equivalent sampling | 200ps |
| Pulse repetition period by equivalent sampling | 0.125s |
| ADC real-time sampling rate | 400KSa/s |

the ground. In these experiments, the volunteer maintained normal breathing, normal heartbeat and stood upright towards the radar.

### B. RESULTS ANALYSIS

#### 1) SIGNAL PREPROCESSING PERFORMANCE

in this section, signal preprocessing performance is discussed based on the data from the first experiment. Figure 8(a) is the radar raw data. Figure 8(b) shows the results after removing the DC component, static clutter and linear trend. The simulated signal is relatively weak. The results obtained by employing agc are shown in Figure 8(c). The results processed by the filers in slow time and fast time are given in Figure 8(d). The life signal is gradually enhanced in the echo matrix compared with the result shown in Figure 8(a).

#### 2) VITAL SIGN SIGNAL EXTRACTION PERFORMANCE AT DIFFERENT DISTANCES IN OUTDOOR AND INDOOR SCENES

In this section, the data acquisition from the second and third experiments is used to evaluate the vital sign signal extraction performance of the proposed algorithm. Figures 9(a), 9(b), 10(a), 10(b), 11(a) and 11(b) show the radar matrix after preprocessing with the human target at 5 meters, 9 meters (under the through-wall condition), 7 meters and their corresponding permutation entropy. As shown in the Figures 9(b), 10(b) and 11(b), the PE value in the nontarget region is higher (approximately 0.8-1), and the PE value in the target region is lower (approximately 0.5-0.75). The PE value in the nontarget region is higher because, in the slow-time dimension of the radar-received echoes, the signal complexity of the target region differs from that of the nontarget region and the human breathing and heartbeat signal is certain and more regular than the background noise; therefore, the corresponding PE value is low, and is thus consistent with the physical meaning of the PE value. The estimated range is 4.89 meters, 9.03 meters, 6.90 meters, and the corresponding measurement error is 0.11 meters,0.03 meters and 0.10 meters.

To explore the extraction performance of the human life signal by the proposed algorithm, take the data of the target at 7 meters as an example. Signals of the human target in adjacent distance gates were selected and combined according to permutation entropy. The combined signal is shown in Figure 11(c) and decomposed into several IMFs by EEMD. The energy ratio of each of the IMFs is shown in Figure 11(d); the energy ratios indicate that the respiration signal is reconstructed by IMF2 and IMF3 and the heartbeat signal is reconstructed by IMF1. Figure 11(e),11(f),11(g), and 11(h) show the reconstructed respiratory and heartbeat signals and corresponding frequency. Table 3 summarizes the results of the proposed algorithm and referenced algorithms, such as fast Fourier transforms algorithm (FFT) [32] and variational mode decomposition algorithm (VMD) [33]. Experimental results show that the proposed algorithm can obtain the vital sign signals and parameters faster than other similar methods.

**TABLE 3. The results compared with the referenced algorithm.**

| Algorithm | Results | 5m | 7m | 9m* |
|---|---|---|---|---|
| FFT | RF (Hz) | 0.42Hz | 0.39Hz | 0.41Hz |
| | HF (Hz) | 1.218Hz | 1.27Hz | 1.30Hz |
| | Observation Time (Seconds) | Approximately 20s | Approximately 20s | Approximately 20s |
| VMD | RF (Hz) | 0.42Hz | 0.39Hz | 0.40Hz |
| | HF (Hz) | 1.23Hz | 1.29Hz | 1.28Hz |
| | Observation Time (Seconds) | 30s | 30s | 30s |
| Proposed Algorithm | RF (Hz) | 0.3906Hz | 0.3906Hz | 0.3906Hz |
| | HF (Hz) | 1.203Hz | 1.313Hz | 1.313Hz |
| | Estimated Distance (Meters) | 4.89m | 6.9m | 9.03m |
| | Observation Time (Seconds) | 10s | 10s | 10s |

RF: Respiratory Frequency
HF: Heartbeat Frequency
9m* means the experiment carried out in through-wall condition.

## V. CONCLUSION

In this paper, we propose an UWB radar vital sign signal extraction algorithm based on permutation entropy and an EEMD algorithm. The distance between the UWB radar and the human target is obtained by calculating the PE value of the radar-received pulse accumulated in slow time. To improve the efficiency of the UWB radar, the signals of the target distributed in adjacent distance gates are selected and combined based on PE. The recombined signal is adaptively decomposed by the EEMD algorithm, and the respiratory and heartbeat signal are reconstructed in the time domain. Experimental results show that the proposed algorithm can effectively separate the life signal from clutter; therefore, the algorithm is suitable for rapid extraction of vital sign signals and corresponding parameters. Further, compared with the other algorithms mentioned in Table 3, the proposed algorithm integrates the life signals of adjacent distance gates, so the required observation time is approximately 1-2 times shorter.

## VI. ACKNOWLEDGMENT

The author would like to thank the editor and anonymous reviewers for their valuable ideas, time, and suggestions for improving the quality of the manuscript.

## REFERENCES

[1] J. Kranjec, S. Beguš, J. Drnovšek, and G. Geršak, "Novel methods for noncontact heart rate measurement: A feasibility study," *IEEE Trans. Instrum. Meas.*, vol. 63, no. 4, pp. 838–847, Apr. 2014.
[2] J. Tu and J. Lin, "Fast acquisition of heart rate in noncontact vital sign radar measurement using time-window-variation technique," *IEEE Trans. Instrum. Meas.*, vol. 65, no. 1, pp. 112–122, Jan. 2016.
[3] J. Li, L. Liu, Z. Zeng, and F. Liu, "Advanced signal processing for vital sign extraction with applications in UWB radar detection of trapped victims in complex environments," *IEEE J. Sel. Topics Appl. Earth Observat., Remote Sens.*, vol. 7, no. 3, pp. 783–791, May 2014.
[4] Z. Li, W. Li, H. Lv, Y. Zhang, X. Jing, and J. Wang, "A novel method for respiration-like clutter cancellation in life detection by dual-frequency IR-UWB radar," *IEEE Trans. Microw. Theory Techn.*, vol. 61, no. 5, pp. 2086–2092, May 2013.
[5] J. W. Choi, D. H. Yim, and S. H. Cho, "People counting based on an IR-UWB radar sensor," *IEEE Sensors J.*, vol. 17, no. 17, pp. 5717–5727, Sep. 2017.
[6] J. W. Choi, S. H. Cho, Y. S. Kim, N. J. Kim, S. S. Kwon, and J. S. Shim, "A counting sensor for inbound and outbound people using IR-UWB radar sensors," in *Proc. IEEE Sensors Appl. Symp. (SAS)*, Apr. 2016, pp. 528–532.
[7] X. Yang, W. Yin, L. Li, and L. Zhang, "Dense people counting using IR-UWB radar with a hybrid feature extraction method," *IEEE Geosci. Remote Sens. Lett.*, vol. 16, no. 1, pp. 30–34, Jan. 2019.
[8] H. Cho, Y. Park, H. Lyu, and J. Cho, "Novel heart rate detection method using UWB impulse radar," *J. Signal Process. Syst.*, vol. 87, no. Apr. 2016, pp. 229–239, 2017.
[9] X. Liang, H. Zhang, G. Fang, S. Ye, and T. A. Gulliver, "An improved algorithm for through-wall target detection using ultra-wideband impulse radar," *IEEE Access*, vol. 5, pp. 22101–22118, 2017.
[10] S. Singh, Q. Liang, D. Chen, and L. Sheng, "Sense through wall human detection using UWB radar," *EURASIP J. Wireless. Commun. Netw.*, vol. 2011, no. 20, pp. 1–11, Jun. 2011.
[11] Y. Xu, S. Dai, S. Wu, J. Chen, and G. Fang, "Vital sign detection method based on multiple higher order Cumulant for ultrawideband radar," *IEEE Trans. Geosci. Remote Sens.*, vol. 50, no. 4, pp. 1254–1265, Apr. 2012.
[12] L. Liu, Z. Liu, H. Xie, B. Barrowes, and A. C. Bagtzoglou, "Numerical simulation of UWB impulse radar vital sign detection at an earthquake disaster site," *Ad Hoc Netw.*, vol. 13, pp. 34–41, Feb. 2014.
[13] L. Liu, Z. Liu, and B. E. Barrowes, "Through-wall bio-radiolocation with UWB impulse radar: Observation, simulation and signal extraction," *IEEE J. Sel. Topics Appl. Earth Observ. Remote Sens.*, vol. 4, no. 4, pp. 791–798, Dec. 2011.
[14] A. Nezirovic, A. G. Yarovoy, and L. P. Ligthart, "Signal processing for improved detection of trapped victims using UWB radar," *IEEE Trans. Geosci. Remote Sens.*, vol. 48, no. 4, pp. 2005–2014, Apr. 2010.
[15] P. S. Feng Jiuchao, "Extraction algorithm of vital signals based on empirical mode decomposition," *J. South China Univ. Technol. Sci. Ed.*, vol. 38, no. 10, pp. 1–6, 2010.
[16] L. Jiang, H. Wei, S. Guan, and L. Che, "A study on UWB vital signal detection method based on EEMD and HOC," *Mod. Radar*, vol. 37, no. 5, pp. 25–30, 2015.
[17] X. Hu and T. Jin, "Short-range vital signs sensing based on EEMD and CWT using IR-UWB radar," *Sensors*, vol. 16, no. 12, pp. 2025–2042, 2016.
[18] J. Yan, H. Hong, H. Zhao, Y. Li, C. Gu, and X. Zhu, "Through-wall multiple targets vital signs tracking based on VMD algorithm," *Sensors*, vol. 16, no. vol. 8, p. 1293, Aug. 2016.
[19] Y. Xu, S. Wu, C. Chen, J. Chen, and G. Fang, "A novel method for automatic detection of trapped victims by ultrawideband radar," *IEEE Trans. Geosci. Remote Sens.*, vol. 50, no. 8, pp. 3132–3142, 2012.
[20] X. Liang, H. Zhang, S. Ye, G. Fang, and T. A. Gulliver, "Improved denoising method for through-wall vital sign detection using UWB impulse radar," *Digit. Signal Process. A Rev. J.*, vol. 74, pp. 72–93, 2018.
[21] X. Liang, J. Deng, H. Zhang, and T. A. Gulliver, "Ultra-wideband impulse radar through-wall detection of vital signs," *Sci. Rep.*, vol. 8, no. 1, p. 13367, 2018.
[22] J. Rovňaková and D. Kocur, "Weak signal enhancement in radar signal processing," in *Proc. 20th Int. Conf. Radioelektronika*, Apr. 2010, pp. 147–150.
[23] L. Shen, D.-H. Kim, J.-H. Lee, H.-M. Kim, P.-J. Park, and H. K. Yu, "Human detection based on the excess kurtosis in the non-stationary clutter enviornment using UWB impulse radar," in *Proc. 3rd Int. Asia–Pacific Conf. Synth. Aperture Radar (APSAR)*, Sep. 2011, pp. 1–4.
[24] S. D. Liang, "Sense-through-wall human detection based on UWB radar sensors," *Signal Process.*, vol. 126, pp. 117–124, 2016.
[25] C. Bandt and B. Pompe, "Permutation entropy: A natural complexity measure for time series," *Phys. Rev. Lett.*, vol. 88, no. 17, p. 4, 2002.
[26] S. Nalband, A. Prince, and A. Agrawal, "Entropy-based feature extraction and classification of vibroarthographic signal using complete ensemble empirical mode decomposition with adaptive noise," *IET Sci., Meas. Technol.*, vol. 12, no. 3, pp. 350–359, 2017.
[27] M. Riedl, A. Müller, and N. Wessel, "Practical considerations of permutation entropy: A tutorial review," *Eur. Phys. J. Spec. Top.*, vol. 222, no. 2, pp. 249–262, 2013.
[28] Z. Chen, Y. Li, H. Liang, and J. Yu, "Improved permutation entropy for measuring complexity of time series under noisy condition," *Complexity*, vol. 2019, pp. 1–12, Mar. 2019.
[29] C. Bandt, "A new kind of permutation entropy used to classify sleep stages from invisible EEG microstructure," *Entropy*, vol. 19, no. 5, pp. 197–208, 2017.
[30] N. E. Huang, "The empirical mode decomposition and the Hubert spectrum for nonlinear and non-stationary time series analysis," *Proc. R. Soc. A Math. Phys. Eng. Sci.*, vol. 454, no. 1971, pp. 903–995, 1998.
[31] W. U. Zhaohua and N. E. Huang, "Ensemble empirical mode decomposition: A noise-assisted data analysis method," *Adv. Adapt. Data Anal.*, to be published.
[32] N. I. A. Sheng *et al.*, "Non-contact life-parameters signal detecting of frequency domain signal integration based on FFT," vol. 24, no. 2, pp. 172–175, 2003.
[33] C. Ding, J. Yan, L. Zhang, H. Zhao, H. Hong, and X. Zhu, "Noncontact multiple targets vital sign detection based on VMD algorithm," in *Proc. IEEE Radar Conf.*, May 2017, pp. 0727–0730.

**DEGUI YANG** was born in 1978. He received the B.S., M.S., and Ph.D. degrees from the Electronic Science and Engineering School, National University of Defense Technology, China, in 1997, 2002, and 2011, respectively. He is currently a Professor with the School of Aeronautics and Astronautics, Central South University, Changsha, China. From 2016 to 2017, he was an Academic Visitor of the Imperial College London, U.K. His research interests include the optical and radar characteristic analysis, and radar signal processing.

**ZHENGLIANG ZHU** received the B.S. degree from the Changsha University of Science and Technology, Changsha, China, in 2017. He is currently pursuing the master's degree with the School of Aeronautics and Astronautics, Central South University, Changsha. His current research interests include UWB radar signal processing and deep learning.

**BUGE LIANG** received the B.S. and Ph.D. degrees from the Electronic Science and Engineering School, National University of Defense Technology, China, in 2001 and 2007, respectively. He is currently a Professor with the School of Aeronautics and Astronautics, Central South University, Changsha, China. His research interests include high power nanosecond pulsers, UWB radar, and signal processing.